

Combined Electrical Resistivity Tomography (ERT), Direct-Push Electrical Conductivity (DP-EC) Logging and Coring – A New Methodological Approach in Geoarchaeological Research

PETER FISCHER^{1*}, TINA WUNDERLICH², WOLFGANG RABEL²,
ANDREAS VÖTT¹, TIMO WILLERSHÄUSER¹, KALLIOPI BAIKA³,
DIAMANTO RIGAKOU⁴ AND GARYFALIA METALLINO⁴

¹ Institute for Geography, Johannes Gutenberg-Universität Mainz, Johann-Joachim-Becher-Weg 21, 55099 Mainz, Germany

² Institute of Geosciences, Department of Geophysics, Christian-Albrechts-Universität zu Kiel, Otto-Hahn-Platz 1, 24118 Kiel, Germany

³ Centre Camille Jullian, Aix-Marseille Université, MMSH, 5, rue du Château de l'Horloge, 13094 Aix-en-Provence, France

⁴ Eighth Ephorate of Prehistoric and Classical Antiquities, Armeni Vraila 1, 49100 Corfu, Greece

ABSTRACT Non-invasive geophysical methods have been increasingly applied in geoarchaeological research commonly showing the need of data calibration based on stratigraphical information deduced from outcrops or sediment cores. In this contribution, a methodological approach combining two-dimensional (2D) electrical resistivity tomography (ERT) and stratigraphical data based on coring and, for the first time in geoarchaeological research, direct-push electrical conductivity (DP-EC) logging is presented and discussed. The approach yields high resolution data based on studies of two different types of archives, the Holsterburg site in central Germany located in a fluvio-terrestrial zone and the Corfu City site in Greece located in a near-coastal zone. It is shown that DP-EC logs trace fluctuations over grain size in high resolution which reflect changes of depositional conditions in the course of time. In addition, constraints from DP-EC logs in the form of layer interfaces and electrical resistivities were incorporated into the ERT inversion process minimizing the ambiguity of inversion results. It is shown that incorporating regions with certain starting resistivities based on DP-EC logs exceed the advantage of using layer interfaces alone. It is concluded that in future geoarchaeological and geomorphological studies a combined application of coring, DP-EC logging and ERT measurements should be considered as a standard approach towards a more comprehensive stratigraphical characterization of the shallow subsurface. Copyright © 2016 John Wiley & Sons, Ltd.

Key words: electrical resistivity tomography; direct-push EC logging; coring; geoarchaeology; geomorphology; Holsterburg lowland castle (central Germany); Corfu Island (Greece)

Introduction

The application of geoarchaeological methods in archaeological research is of great importance for the understanding of environmental changes and associated

site formation processes. In general, landscape and environmental development depends on natural processes such as earth surface processes, climatic and tectonic factors and associated processes of the overall geomorphic system in different temporal and spatial scales. In addition, human–environmental interaction has played a major role since the Palaeoanthropocene, the period between the first human impacts on natural landscapes and rapidly increasing, anthropogenically

* Correspondence to: P. Fischer, Institute for Geography, Johannes Gutenberg-Universität Mainz, Johann-Joachim-Becher-Weg 21, 55099 Mainz, Germany. E-mail: p.fischer@geo.uni-mainz.de

induced environmental changes caused by industrial and post-industrial societies (Foley *et al.*, 2013). Both naturally triggered and human induced impacts on the environment leave distinct signatures within geological archives associated with distinct processes which can be deciphered by (geo-)archaeological methods.

In recent times, especially non-invasive geophysical methods have been increasingly applied in geoarchaeological research (e.g. Hecht and Fassbinder, 2006; Welham *et al.*, 2014; Rabbel *et al.*, 2015). In this context, the calibration of geophysical data by stratigraphical information deduced from outcrops or sediment cores is an important component of data interpretation (e.g. Seeliger *et al.*, 2013; Fischer *et al.*, 2015). In this contribution, we present a methodological approach combining two-dimensional (2D) electrical resistivity tomography (ERT) and stratigraphical data based on coring and direct-push electrical conductivity (DP-EC) logging. So far, DP-EC logging has been applied mainly in the framework of hydrogeological and geotechnical investigations as it allows for a differentiation of sediment or soil types especially in the saturated zone (Schulmeister *et al.*, 2003; Harrington and Hendry, 2006; Hausmann, 2013). In simple terms, high conductivity (and its inverse, low resistivity) correlates to fine-grained sediments while low conductivity (and thus high resistivity) correlates to coarser grained deposits.

DP-EC logging provides centimetre-scale stratigraphic information in the vertical direction along the drill hole, whereas the horizontal resolution of direct-push surveys is usually much coarser, typically of the order of (some) 10 m, depending on drill hole spacing. In contrast, ERT profiling provides laterally continuous imaging of geological structure, however at a much lower vertical resolution decreasing with target depth. Therefore, in order to optimize near-surface geoelectric prospecting, it is advantageous to combine ERT and DP-EC logging. A visual comparison of ERT images and DP-EC logs yields qualitative results only and interpretation may be even difficult occasionally because of the large differences in vertical resolution. As a step towards an integrative, quantitative data interpretation we suggest incorporating DP-EC logs in the ERT computations as mathematical constraints.

In the present article we apply this 'constrained ERT' to two field examples in order to investigate the potential and effectiveness of this methodological approach, which serves to characterize the structure of the shallow subsurface as a base for reconstructing landscape and environmental changes. The example study sites

are the Holsterburg lowland castle (central Germany) and Corfu City (Greece). Besides serving as methodological test sites these locations are of geoarchaeological interest because they represent two different types of archives: The Holsterburg site comprises archives of the fluvio-terrestrial zone while the Corfu City site is located in the near-coast zone. Both archives are characterized by high groundwater tables which are different in their hydrochemical properties.

The general objectives of our article are based on the following questions:

1. Can DP-EC improve stratigraphic interpretation in addition to sediment coring?
2. Can constrained ERT be used as a tool for interpolating DP-EC logs?
3. Can DP-EC logging be used for improving the resolution of ERT?
4. Is stratigraphic information from coring sufficient for calibrating ERT, or do we need DP-EC explicitly for gaining reliable results?

Besides these methodological aspects we aim at improving the specific geological information on the two example sites by answering the question:

5. Can the combined interpretation of ERT and DP-EC improve the imaging of strata affected by salt-water intrusion?

In the next section the regional setting and open questions of the two example sites are explained followed by the description of applied methods and results by test location. The discussion section explains geoarchaeological implications and puts a special focus of the sensitivity of ERT with respect to deep thin layers.

Regional setting and previous geoarchaeological investigations

Holsterburg lowland castle (central Germany)

The Holsterburg castle (51°28'35.43" N; 9°10'18.01" E, German Grid: 3511926,2; 5704522,2) is located to the southeast of the city of Warburg (North-Rhine Westphalia) in the loess landscape of the so called Warburger Börde and was built by the lords of Holthausen in the late twelfth century (Bulla and Knepe, 2011; Fischer *et al.*, 2015).

The castle is situated on an approximately 150 m wide floodplain of a small creek (the so called Holsterbach, Figure 1) draining a small catchment towards the Diemel River valley. The shallow subsurface

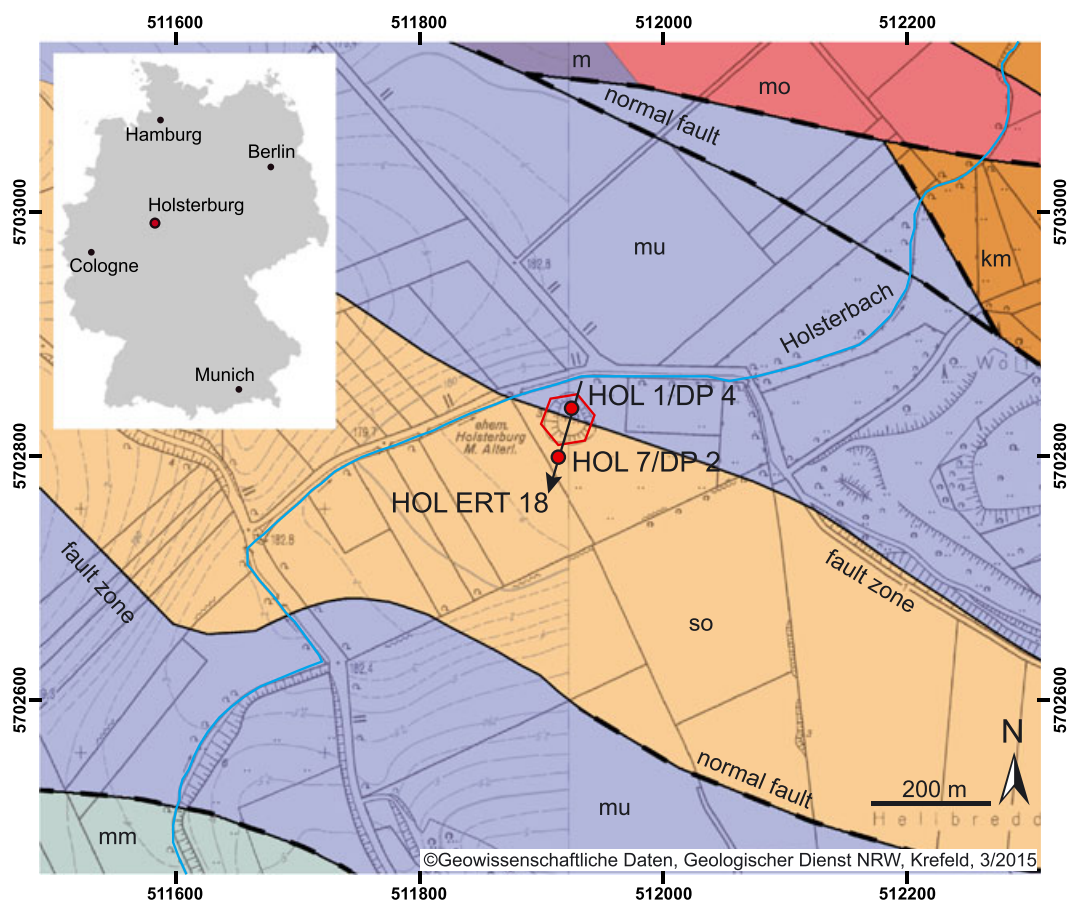


Figure 1. Location of the Holsterburg lowland castle south of Warburg (North Rhine-Westphalia) and locations of cores HOL 1 and HOL 7, direct push HOL DP 2 and HOL DP 4 and electrical resistivity transect HOL ERT 18. Geological units: so: Upper Buntsandstein (Röt formation); m: Muschelkalk (undifferentiated); mu: Lower Muschelkalk (Jena Formation); mm: Middle Muschelkalk; mo: Upper Muschelkalk; km: Middle Keuper. Note that the lowland castle is located directly on top of a fault zone separating the Upper Buntsandstein and the Lower Muschelkalk. Inset: Position of the Holsterburg lowland castle in central Germany. Data source: Digital Geological Map 1:50,000; Geological Survey of North Rhine-Westphalia (Geologischer Dienst NRW, Krefeld, 3/2015); digital topographic map (DTK), Geobasis NRW. This figure is available in colour online at wileyonlinelibrary.com/journal/arp

of the surrounding area is dominated by Pleistocene (mostly Weichselian) loess sediments delivering the parent material for the Late Glacial and Holocene soil formation. Foot slopes and valley bottoms are characterized by Holocene colluvial and alluvial sediments and corresponding soil types. At a larger spatial scale, the study area is located at the north-eastern margin of the Rhenish Slate Mountains (Rheinisches Schiefergebirge) in the transition to the Hessian tectonic basin and the Weser-Leine mountains (Weser-Leine-Bergland). From a geotectonic view, it is characterized by a complex fault system striking from southeast to northwest and which is named Warburg Fault Zone (WFZ, Warburger Störungszone, Meiburg, 1982; Fischer *et al.*, 2015). Within this fault system and adjacent tectonic plates, a stratigraphical sequence from the Lower Triassic (Röt Formation) to the Lower Jurassic (Pliensbachian) occurs. It is known that the entire fault system is situated on top of salt diapirs

(sodium chloride, NaCl) of the Werra series of the Zechstein period (Meiburg, 1982; Fischer *et al.*, 2015). The Holsterburg itself is located directly on top of a fault zone separating the Upper Buntsandstein (Röt Formation) and the Lower Muschelkalk below the Quaternary sedimentary cover (Figure 1).

Previous studies in the vicinity of the Holsterburg castle resulted in a detailed reconstruction of the on-site stratigraphical record and the overall landscape and environmental evolution based on ERT measurements, coring as well as geochemical and archaeobotanical analyses (Meurers-Balke *et al.*, 2014; Fischer *et al.*, 2015). It was shown that the castle was built on a construction layer that was founded on Holocene colluvial and alluvial deposits. This is in contrast to previous assumptions that the castle was built on fluvial gravel of Weichselian age. In addition, geochemical analyses and ERT measurements revealed that

salt-enriched groundwater upwelling occurs directly below the castle bound to the tectonic constellation and salt resources in Triassic and Permian bedrocks (Fischer *et al.*, 2015). However, Weichselian fluvial gravel occurs in a deeper stratigraphical position below the colluvial and alluvial cover sediments but their thickness on top of pre-Pleistocene bedrock could not be determined as the auger could not entirely penetrate the gravels. Hence, DP-EC logging and its combination with ERT measurements were conducted in order to obtain information on the deeper stratigraphical record which could not be calibrated against core data.

Corfu City (Ionian Islands, Greece)

The Greek island of Corfu (Greek Kerkyra) is located in the northern Ionian Sea close to the transition to the Adriatic Sea in an exceptional tectonic stress field between the Hellenic Arc and the Cefalonia Transform

Fault (CTF) in the south and continent–continent collision zone of the Apulian and Eurasian plates in the west (Poulos *et al.*, 1999; Sachpazi *et al.*, 2000; Figure 2a, 2b).

Corfu City itself is exposed to the Gulf of Corfu, one of the most prominent quiescent natural harbours in the eastern Mediterranean Sea (Partsch, 1887). Owing to its key geostrategic position along the main navigation and trade routes between Greece and Italy, ancient Corfu was one of the most important naval bases as well as a main commercial centre for centuries (Baika, 2014). As a colony, the city of ancient Corfu was founded by the Corinthians in the eighth century BC (Bursian, 1872) and subsequently became one of the most significant naval powers of the Archaic and Hellenistic periods.

Despite Corfu's supremacy as naval power and commercial centre, geoarchaeological and palaeogeographical studies focusing on the coastal

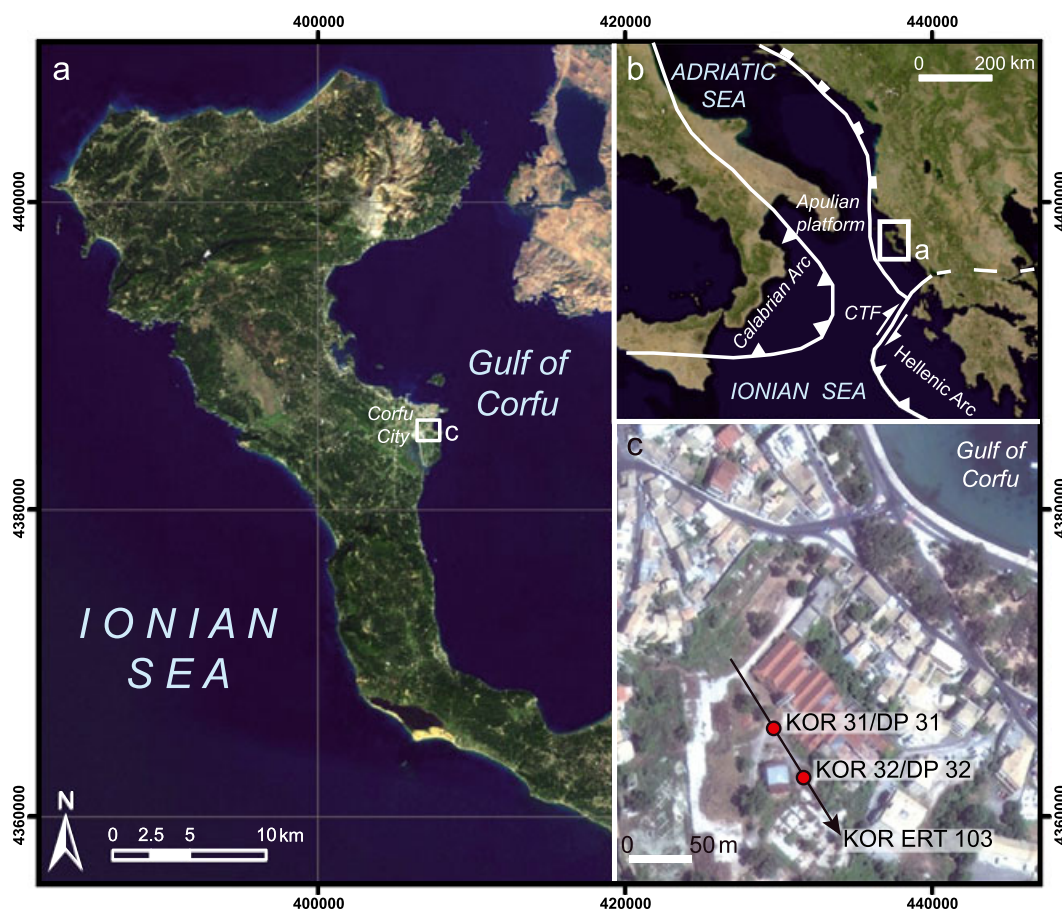


Figure 2. Overview of Corfu Island in the northern Ionian Sea (a) and in the context of the regional tectonic setting in the transition from the Ionian to the Adriatic Sea (b). Detailed view of the study site within Corfu City and locations of cores KOR 31 and KOR 32 and corresponding direct-push electrical conductivity (DP-EC) logs KOR DP 31 and KOR DP 32, and electrical resistivity transect KOR ERT 103 (c). The study site is located in a former factory site approximately 200 m southwest of the recent coastline (source: Microsoft BING maps, access 2015-02-19). This figure is available in colour online at wileyonlinelibrary.com/journal/arp

development and its relevance for evolving cultural landscapes are not available so far. Changes in the coastline configuration were crucial for the city at least since antiquity as ancient harbour installations are found today 250–300 m distant from the sea (Baika, 2014). The study area is located in a former factory site in the northern part of the ancient city where no information with regards to the shallow subsurface was available prior to the investigations presented here.

Previous geoarchaeological studies on Corfu Island focus on the general relationship between palaeogeographical and cultural evolution during the Holocene including coastline changes and fluctuations of the relative sea level. In this context, local geological archives on Corfu Island offer ideal preconditions such as a variety of stratigraphical units and a cultural tradition rich in material artefacts. Our study focusses on distinct shifts in depositional conditions associated with palaeogeographical evolution. DP-EC logging was used to gain additional information on the stratigraphical record and to refine inversion results of ERT measurements, especially in saltwater-saturated strata.

Methods

We combined geophysical and sedimentological methods in order to decipher local stratigraphies and environmental changes within the available archives around the Holsterburg site and in Corfu City. ERT measurements were conducted using a multi-electrode device (type Syscal R1 Plus Switch 48, Iris Instruments) and a Wenner-Schlumberger electrode array with 48 electrodes and 2 m (Holsterburg) and 3 m (Corfu City) spacing. ERT inversion was carried out in 2D by applying BERT (Boundless Electrical Resistivity Tomography, Günther *et al.*, 2006), a software based on finite-element (FE) modelling. The subsurface model consists of triangular cells that are small at the surface and become larger towards greater depths. The increase of cell size corresponds to the decrease of structural resolution of ERT with depth. The use of a FE grid enables modelling of topography in an easy and exact way. ERT measurements performed at the earth's surface generally suffer from resolution limits that are caused by a physical uncertainty relation between size and electric conductivity of subsurface structure. Therefore, ERT results can be improved by constraining the tomographic computations through drilling results. For example, the DP-EC logs provide the depths of interfaces and electrical resistivities of layers that can be incorporated as numerical

constraints in the ERT inversion process. Technically, this can be achieved in different ways (Günther and Rücker, 2006). A simple way is to alter the triangle mesh in such a way that cell boundaries match layer boundaries. Then a weight is assigned to each boundary of neighbouring cells steering the allowed smoothness of change of resistivities across the interfaces. If a layer boundary is assumed to lie between two model cells, the resistivities of these cells are allowed, but not forced, to increase or decrease independently from each other during the computation. In addition, starting values of electrical resistivity can be assigned to specific regions of the subsurface model. In the iterative ERT computations these starting values are usually changed in order to fit the data, but a weight can be used to limit the allowed deviation from the starting value in order to fulfil the constraints of the drilling. These constraint regions can be completely decoupled from the neighbouring area or coupled to varying degrees depending on strictness with which the user wishes to extend the constraint into the area off the borehole.

The quality of the fit of the resulting electrical resistivity model is given by the RRMS (relative root mean square) deviation between measured and modelled data (in %) and by the chi-squared misfit. Günther *et al.* (2006) state that chi-squared values of one to five show that results are statistically reliable meaning that the data are neither overfitted nor underfitted.

Coring was conducted using a drill rig (type Nordmeyer RS 0/2.3) and steel auger with core diameters between 80 and 60 mm (Figure 3). Sediment cores were cleaned, photo-documented and recorded by sedimentological and geomorphological methods (Ad-hoc-AG Boden, 2005). Position and elevation of coring sites and ERT measurements were measured using a differential global positioning system (DGPS) (type TOPCON HiPerPRO). Parallel to coring DP-EC logging was achieved using a Geoprobe SC520 soil conductivity probe. According to Schön (2004) electrical conductivity in unconsolidated sediments is mainly controlled by sediment mineralogical characteristics, moisture content and the chemical composition of the pore water. In saturated sediments below ground water table, electrical conductivity logs yield direct evidence of changes in sedimentary characteristics if variations in pore water chemical composition are negligible (Schulmeister *et al.*, 2003; Harrington and Hendry, 2006). In general, higher electrical conductivities typically represent finer grained sediments, such as silt and clay, while sand and gravel have distinctively lower conductivities (e.g. Wunderlich *et al.*, 2013). Ionic contaminants can increase the



Figure 3. Excavation site of the Holsterburg lowland castle (black arrow) in the loess landscape of the Warburger Börde (a). The city of Warburg is visible in the background of the picture. Nordmeyer RS 0/2.3 drill rig with mounted Geoprobe DP-EC logging unit conducting HOL 4 within the castle (b). Geoprobe Field Instrument logging electrical conductivity and rate of penetration data as well as pushing depth (c) (photographs: A. Vött, July 2014). This figure is available in colour online at wileyonlinelibrary.com/journal/arp

conductivity of the soil (Direct Image, 2008). The electrical conductivity probe that was used is composed of four electrodes in linear arrangement and was operated in a Wenner electrode array enabling a vertical resolution of 0.02 m (www.geoprobe.com; Harrington and Hendry, 2006). The system measures electrical current and voltage constantly with depth used for a calculation of electrical conductivity. The specific conductivity is the quotient between current and voltage multiplied by a constant depending on the electrode geometry. The resulting unit is milli-Siemens per meter (mS/m) (Direct Image, 2008). Inverse values of electrical conductivity are defined as electrical resistivity. Grain size analyses were conducted for 52 samples of core KOR 31 from the Corfu City site following the sieve and pipette method after Köhn (DIN ISO 11277, 2002).

The ERT results are expected to give information about the resistivity distribution of the subsurface over a profile, whereas the coring data and DP-EC logs only represent point information. Nevertheless,

the coring data and DP-EC logs yield very high vertical resolution that could help in improving the ERT results, which lack vertical resolution (at least compared to the DP-EC logs).

Results

Holsterburg lowland castle

Lithostratigraphical results based on coring and DP-EC loggings are summarized in Figure 4. While core HOL 1 was drilled inside the castle close to the northern curtain wall, coring site HOL 7 is located outside the castle in the direct southern periphery (Figure 1). The base of both cores consists of fluvial gravel most likely correlating with the Weichselian Lower Terrace. In core HOL 1, this gravel is covered by Late Glacial to Early Holocene overbank deposits dominated by silt (Fischer *et al.*, 2015). In core HOL 7, these greenish-grey overbank deposits are

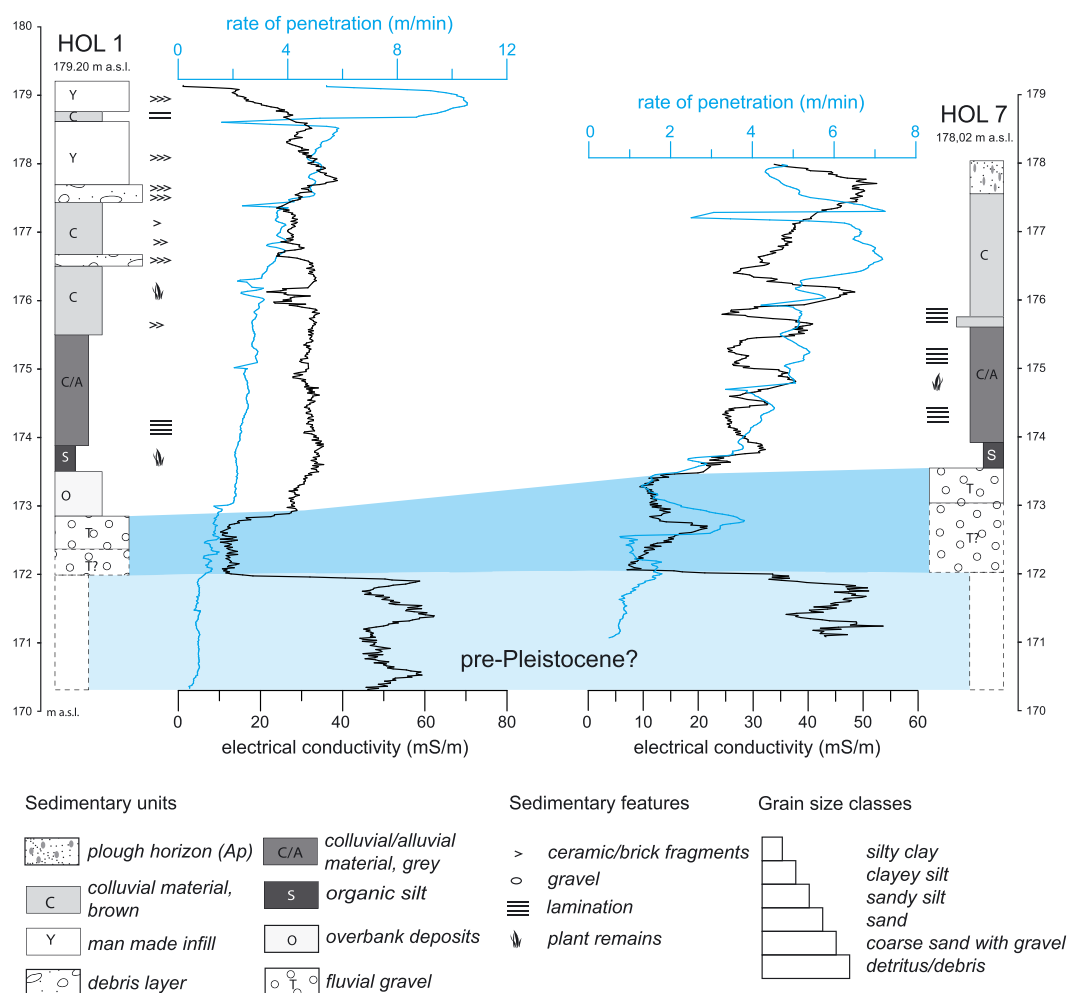


Figure 4. Stratigraphical composition, EC (electrical conductivity) and ROP (rate of penetration) data of core HOL 1/DP 4 conducted inside the castle and core HOL 7/DP 2 drilled to the south of the castle (cf. Figure 1). Grain size classification is based on detailed field description of the cores. Upper shading indicates transition from fine-grained colluvial and alluvial deposits to fluvial gravel. The upper limit of the gravel unit fits with stratigraphical data derived from coring. The lower shading indicates the transition to pre-Pleistocene bedrock most likely consisting of clay-dominated Upper Buntsandstein (Röt). This stratigraphic boundary was not detected by coring, but is clearly seen in the electrical conductivity data. This figure is available in colour online at wileyonlinelibrary.com/journal/arp

missing. The fluvial gravel consists of poorly rounded limestone and sandstone clasts indicating short distance transport by the Pleistocene ancestor of the Holsterbach. Dark grey to blackish clay, rich in silt, accumulated on top of the Pleistocene sedimentary sequence showing no remains of anthropogenic influence. On top, greyish laminated, clayey silt partially enriched in plant remains accumulated indicating a colluvial and/or alluvial depositional environment. Ceramic and limestone fragments encountered in the lower part of the colluvial/alluvial deposits indicate human activities. The sequence is complemented by colluvial sediments of brownish silt overlain by anthropogenic infill in core HOL 1. The construction

level of the castle is indicated in core HOL 1 by limestone fragments and gravel at 176.4 m above sea level (a.s.l.). The debris layer further up core is interpreted as a destruction layer as it occurs in the post-castle infill. The groundwater table was located at approximately 175.5 m a.s.l. and water table height showed only minor fluctuations in all cores. In view to the DP-EC data, the rate of penetration (ROP) clearly shows decreasing values towards the base of both profiles indicating increasing bulk density of the deposits. In core HOL 1, electrical conductivity in the anthropogenically influenced upper part of the sequence reveals minor fluctuations while especially silt-dominated colluvial and alluvial deposits turn out to be relatively homogeneous.

In contrast, comparable deposits in core HOL 7 yield alternating electrical conductivity values indicating a typical colluvial to alluvial depositional environment characterized by interbedded strata of slightly coarser and finer grain sizes.

This alternation fits well with observed lamination in the sediment core. The transition from silt-dominated colluvial and alluvial deposits to the underlying fluvial gravel is traced by distinctly decreasing electrical conductivity values. In direct-push HOL 2 intercalated finer grained sediments within the gravel unit are indicated by a peak in electrical conductivity at 172.5 m a.s.l. Stratigraphy explicitly is changing in an elevation of 172 m a.s.l. indicated by strongly increasing electrical conductivity values in both cores accompanied by the lowest ROP values found within the whole sequence.

The unconstrained ERT inversion results of HOL ERT 18 (Figure 5a) clearly show the remains of the castle by high electrical resistivity at the surface. Underneath, no clear layering such as indicated by the core data is visible. Below the Holsterburg, the resistivities

decrease to $< 10 \text{ } \Omega\text{m}$ indicating fine-grained material and/or increasing (salt) water content. Although there is a slight increase in resistivity in the lower part between $x=70\text{--}90 \text{ m}$, the resistivity value of the coarse-grained fluvial gravel, as shown by the DP-EC log, is not resolved. This is not surprising because the thickness of the layer is too small (*c.* 1 m) compared to its depth (4–6 m) for being resolved by surface-based ERT. However, by performing a constraint inversion, we can test (1) whether or not the assumption that the gravel layer extends along the whole profile is in accordance with the geoelectric data, and (2) if yes: whether or not this layer is likely to be homogeneous in terms of electrical resistivity.

The corresponding computation shows that the assumption of a continuous gravel layer leads to similar RRMS error and the chi-squared misfit as the unconstrained inversion (Figure 5b). The resistivities in this layer were initialized constantly with $76 \text{ } \Omega\text{m}$ (i.e. the mean of the DP-EC logs in this layer) and were allowed to vary to a limited degree from this starting

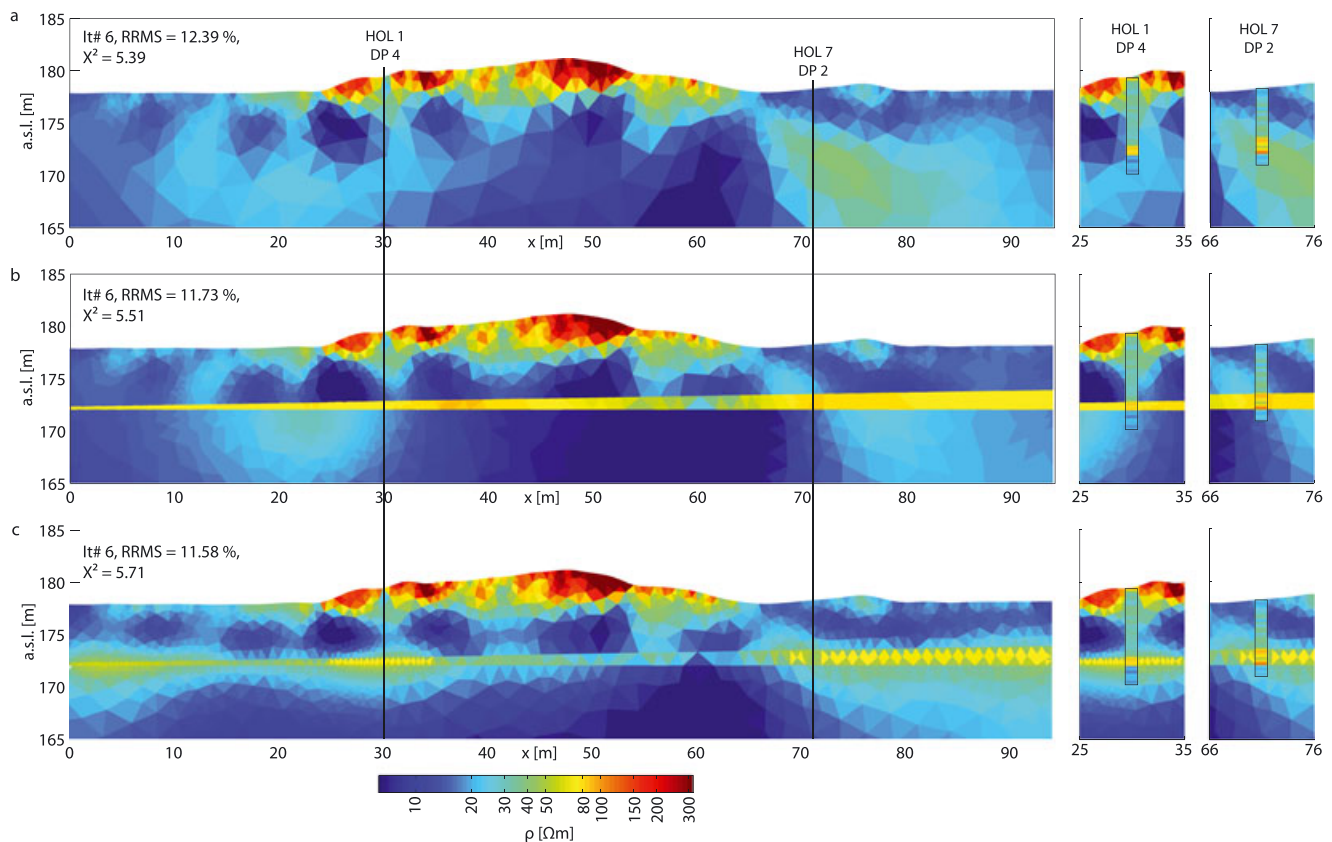


Figure 5. Electrical resistivity tomography (ERT) inversion results of HOL ERT 18 and comparison with direct-push electrical conductivity (DP-EC) logs that were converted to electrical resistivity. (a) Unconstrained inversion (damping factor $\lambda=20$). (b) Inversion with top and bottom of gravel layer incorporated as interfaces and starting resistivity of $76 \text{ } \Omega\text{m}$ for this layer (damping factor $\lambda=20$). (c) Inversion with gravel layer region of starting resistivity $76 \text{ } \Omega\text{m}$ and coupling to surrounding region (damping factor $\lambda=20$). This figure is available in colour online at wileyonlinelibrary.com/journal/arp

value during the iterative tomographic inversion. The resistivities of the gravel layer ended up in the range 24–90 Ωm . Especially at $x=60\text{m}$, the values decrease strongly, which could be explained by (salt) water rise through the known fault system. The resistivity variation of the assumed continuous gravel layer gets even smoother and more variable if the interface constrained is relaxed by lowering the corresponding weights (Figure 5c). In this case, the tomographic inversion results in somewhat extended areas of slightly increased resistivity (20–40 Ωm) that surround the gravel layer. But a distinct change of resistivity across the layer interfaces is still maintained. The local resistivity minimum in the gravel layer at $x=60\text{m}$ is also still present, but is even further smoothed out to the sides. RRMS error and chi-square misfit are again of the same order as in the previous inversion runs, the RRMS error is 1% smaller than for the unconstrained inversion though.

In summary, it can be concluded that an assumed lateral continuity of the gravel layer found in the sediment cores and DP-EC logs does not contradict ERT. However, despite all constraints, the ERT computations lead to a pronounced minimum of electric resistivity (at coordinate $x=60\text{m}$) that can be interpreted as an indication of a (salt) water rise above a fault.

Corfu City

The coring site in Corfu City (Figure 2) is located approximately 200 m to the southwest of the recent shoreline in the northern part of the Kanoni Peninsula where the ancient city (Palaiopolis) was located. Lithostratigraphical results based on coring, DP-EC logging and grain size analyses are displayed in Figure 6. Core KOR 31 was drilled to a total depth of 10 m below surface while DP-EC logging was conducted to 18.8 m below surface. The groundwater table was located around recent sea level. Core KOR 31 shows a sedimentary sequence dominated by marine deposits of alternating energy-related facies. In its lower and upper part, fine-grained sediments with increasing silt and clay contents indicate phases of low-energy deposition. Especially the coarser grained medium to high-energetic layers are characterized by large numbers of marine shells and shell debris. Comparing coring results, electrical conductivity and grain size data yield striking results. Below the anthropogenic infill, increased electrical conductivity values correlate with increased clay and silt contents while the coarser grained layer located around recent sea level shows significantly lower values. An additional peak within this layer is displayed in both electrical conductivity data

and grain size distribution, but was not explicitly noticed in the field. Between 1 and 5.2 m below sea level (b.s.l.), increasing electrical conductivity values obviously mirror slightly increasing silt contents.

Based on field description, this part of the record was described as relatively homogenous with alternations in the fine and medium sand fractions. From 5.2 m b.s.l. downward, electrical conductivity values generally reach higher values but the alternation of low, medium and high-energy depositional conditions as observed in the core are still accurately traced. Highest clay contents in a depth of 7.7 m b.s.l. correlate with the absolute maximum of electrical conductivity.

The unconstrained ERT results of KOR ERT 103 (Figure 7a) show a layered structure with a near-surface layer of resistivities $>50\text{ }\Omega\text{m}$. The surface layer extends to variable depths of 5 to 10 m b.s.l. Below this depth resistivities decrease to values between 2 and 15 Ωm . Some highly resistive anomalies are situated at around 0–20 m, 80 m and 100–130 m profile distance reaching to a depth of approximately 10 m b.s.l.. The larger depth extent of these anomalies at the beginning and end of the profile and resistivity structure at maximum depth are not well constrained by data because the chosen electrode configuration shows only very low sensitivity to resistivity variation in these parts of the profile. Therefore, we concentrate on the central part of the profile in the following sections.

The comparison of ERT and DP-EC results from two boreholes (Figure 7a, right) shows that resistivity values match well at location KOR 32 but show major differences at KOR 31. Therefore, we try to recalibrate the ERT results by applying constraints deduced from core and DP-EC data in different steps. In a first step, we define layer interfaces at the borehole locations across which resistivity smoothing is forbidden during the ERT computation (Figure 7b, white lines). This case corresponds to the assumed situation that only the depths of layer interfaces are known from drilling, but local resistivity values are not. These layer interfaces were derived from drill core inspection (Figure 7). The corresponding ERT result is shown in Figure 7b. The result is similar to the unconstrained ERT, but at KOR 31 the initial disagreement of ERT and DP-EC log has become even worse: the layer between the two constrained interfaces is attributed higher resistivities (20–30 Ωm) than beforehand instead of lower. Other disagreements of this ERT version with the DP-EC log are the relatively low resistivities in the upper layer and higher resistivities in the bottom part. This means that constraining only the depth of interface does not lead to model improvement in this case. Therefore, in a next

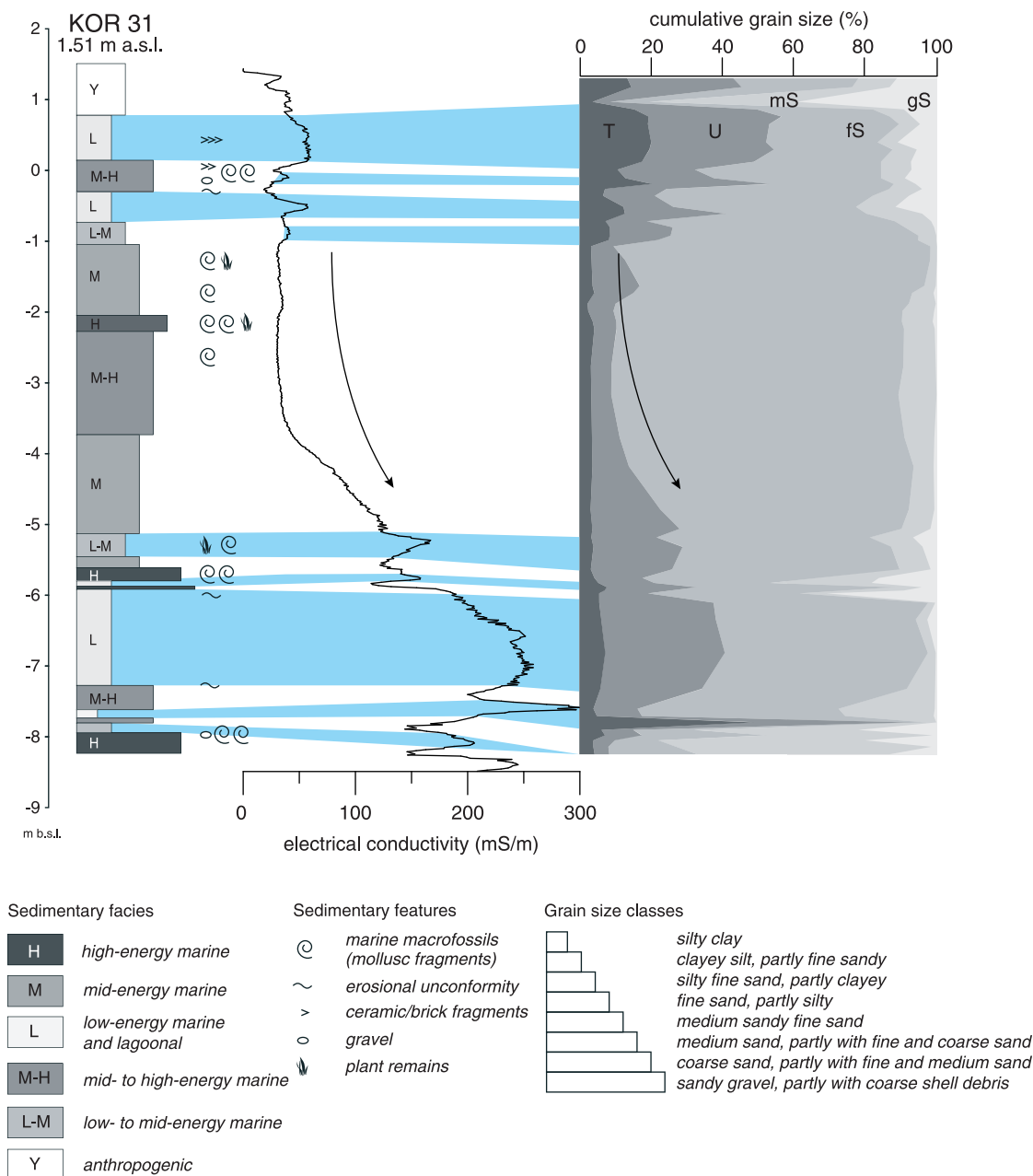


Figure 6. Stratigraphical composition, direct-push electrical conductivity (DP-EC) data and grain size distribution of core KOR 31 drilled in the northern part the ancient city of Corfu. Note that coring had to be stopped due to a collapse of the borehole in a depth of 10 m while DP-EC logging allowed pushing into a depth of 19 m yielding important additional stratigraphical information. Grain size analyses are based on 52 samples taken from the core during fieldwork. Grain size classes: T: clay ($<2\ \mu\text{m}$), U: silt ($2\text{--}63\ \mu\text{m}$), fS: fine sand ($63\text{--}200\ \mu\text{m}$), mS: medium sand ($200\text{--}630\ \mu\text{m}$), gS: coarse sand ($630\text{--}2000\ \mu\text{m}$). Differentiation of depositional environments is based on field description. Electrical conductivity data mirror the stratigraphical composition and the differences in grain sizes in great detail. Blue shading indicates correlation of high electrical conductivity values with maxima in the clay and silt fraction. This figure is available in colour online at wileyonlinelibrary.com/journal/arp

step, the DP-EC results are incorporated in the ERT inversion by constraining both interfaces and resistivity values at the borehole locations (Figure 7c). Starting values were chosen according to the simplified layer model (Figure 8, dashed line) and were allowed to vary only to a certain extent by defining corresponding weights. Additionally,

the segments under constraint were coupled to their surrounding by defining smoothing functions across neighbouring cells. This doubly constrained ERT clearly agrees well with the DP-EC logs (it has to by definition); but the constraining has led to a more plausible ERT structure between the boreholes, too (Figure 8, grey line).

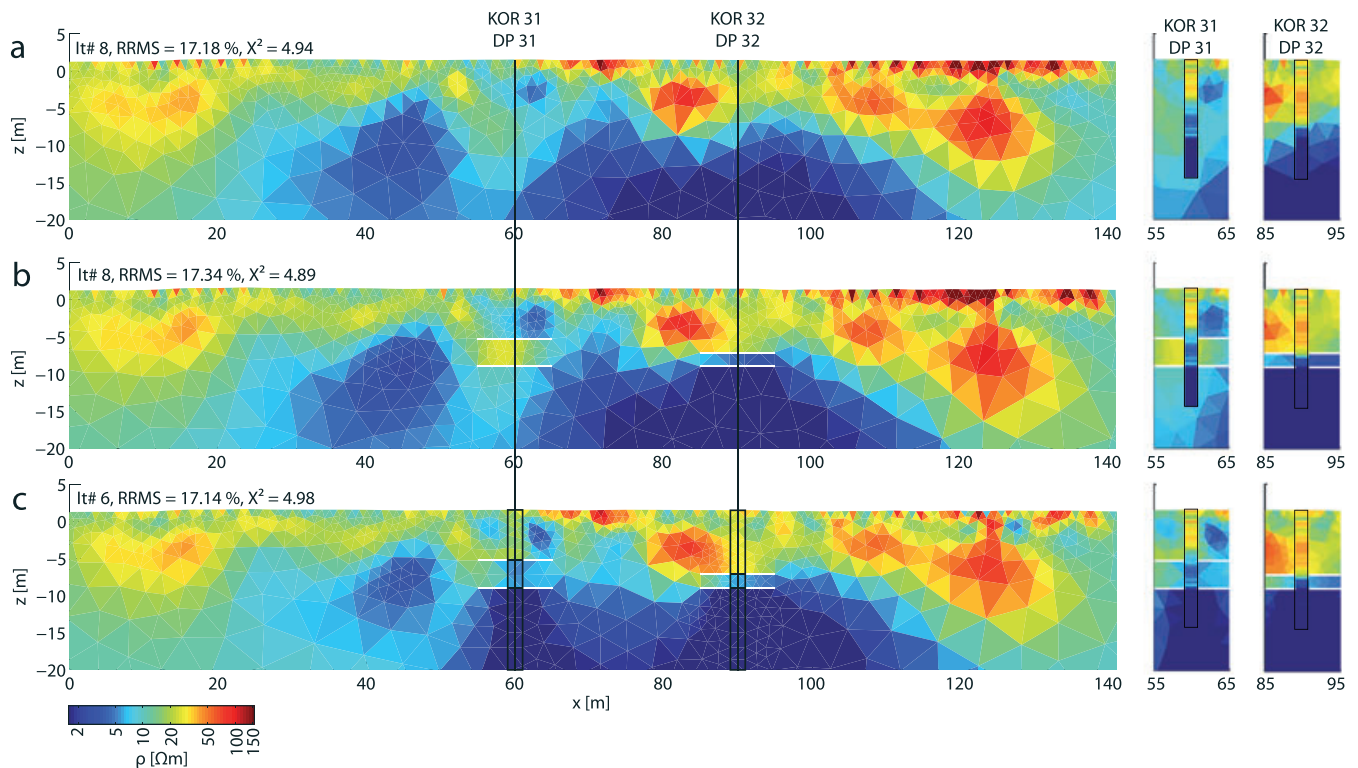


Figure 7. ERT inversion results of KOR ERT 103 and comparison with direct-push electrical conductivity (DP-EC) logs that were converted to electrical resistivity. (a) Unconstrained inversion (damping factor $\lambda = 7$). (b) Inversion with interfaces derived from simplified electrical conductivity logs and cores (damping factor $\lambda = 7$). (c) Inversion with interfaces and regions with specific starting resistivities around the boreholes (damping factor $\lambda = 7$). The regions around the boreholes are coupled to their surroundings. White lines indicate fixed layer interfaces and the regions are marked by black boxes around the coring locations. This figure is available in colour online at wileyonlinelibrary.com/journal/arp

In addition, DP-EC logs were used to compare sedimentary sequences of neighbouring boreholes. In Figure 9, the upper 5 m of core KOR 31 and DP-EC log KOR DP 31 are compared to core KOR 32 and DP-EC log KOR DP 32. Coring site KOR 32 is located 60 m to the southeast of site KOR 31 (Figure 2). Here, we found an intersecting coarse-grained layer just below recent sea level. At its base, this layer is characterized by erosional contacts. DP-EC logs help to clearly define the lower and upper boundaries of this mid-to coarse-sand unit. Depositional conditions below and above this sand layer are clearly different; silt-dominated deposits document low-energy shallow marine to lagoonal environments.

Discussion

Holsterburg

The DP-EC logs yield additional and valuable information on the stratigraphy beyond that of cores. The simplified sequence consisting of silt-dominated colluvial

and alluvial deposits and underlying coarse-grained fluvial deposits is accompanied by information on gravel thickness and a further stratigraphic boundary towards fine-grained sediments at a depth of 172.0 m a.s.l. These fine-grained deposits are characterized by highest conductivity values and lowest rates of penetration indicating the occurrence of dense material, rich in clay, most likely correlating to weathered pre-Pleistocene bedrock representing the local aquiclude. According to the geological map (Figure 1) a correlation to weathered claystones and limestones of the Triassic Röt formation and the Lower Muschelkalk, respectively, is likely. Differences in curve progression of DP-EC logs in HOL 1/DP 4 and HOL 7/DP 2 are most likely due to different compaction rates. DP 4 is located directly below the castle while DP 2 was conducted to the south of the castle and is not directly influenced by the former construction works. Regarding the combination of core and DP-EC data with ERT measurements, one question is if the incorporation of a continuous gravel layer is reasonable, although is not proven for the entire ERT transect by coring or electrical conductivity logging. A total of six cores

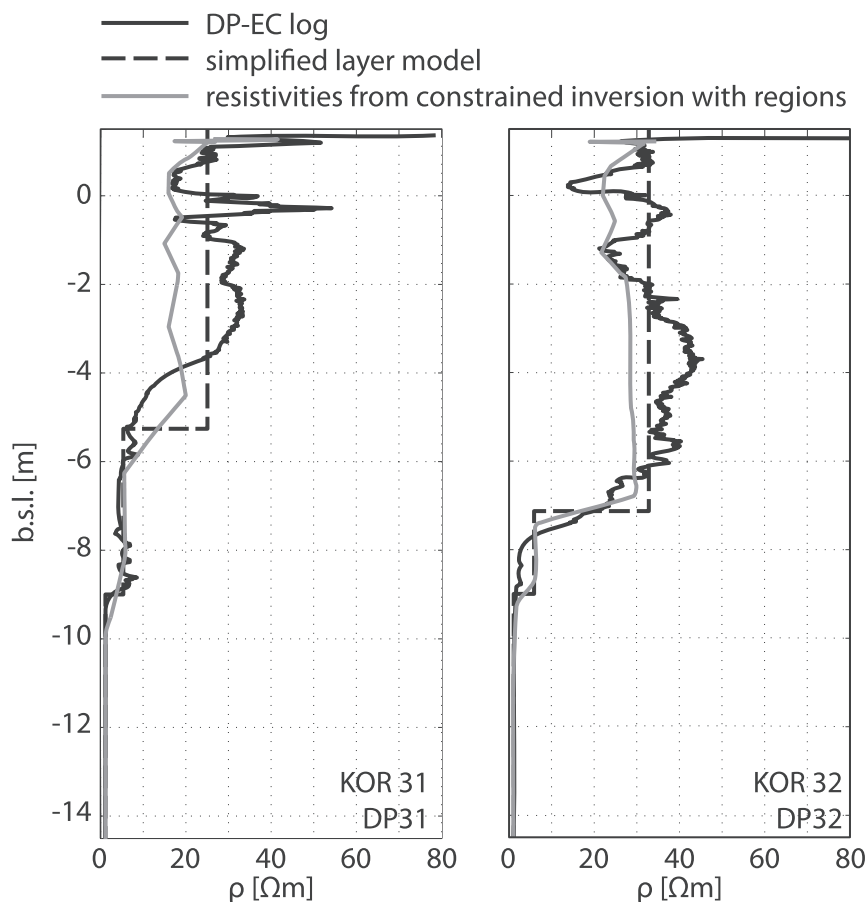


Figure 8. Comparison of direct-push electrical conductivity (DP-EC) with simplified layer model derived from direct-push and cores and the resistivity-depth distribution from the constrained inversion with regions (see Figure 7c). This figure is available in colour online at wileyonlinelibrary.com/journal/arp

was drilled within the alluvial zone in the surrounding of the castle (Fischer *et al.*, 2015). Each of these cores encountered the fluvial gravel indicating extensive accumulation over the entire flood plain.

The constrained ERT results (Figure 5) showed that the assumption of a continuous gravel layer is compatible with the measurements obtained. However, the question has to be asked as to whether the ERT measurements are sensitive at all to this thin layer, which occurs at a comparatively great depth. Therefore, we simulated ERT measurement for theoretical subsurface models consisting of the unconstrained ERT model (Figure 5a) to that a homogeneous layer of constant resistivity was added at the depth of the gravel layer. In three different runs the resistivity of this layer was set to 10, 100 and 1000 Ωm , respectively. The simulated ERT data of these models are shown in the form of resistivity pseudosections in Figure 10. For comparison, the measured pseudosection and the simulated pseudosection for the unconstrained ERT model are also shown. It can

be clearly seen that the layer has a considerable impact on the apparent resistivity values of the pseudosections, so the measurements are sensitive to it in principle. The RRMS differences between the apparent resistivity values of the measured and simulated pseudosections for the different models are shown in Table 1.

The model with a 100 Ωm layer (Model 3 in Table 1) has a similar RRMS error as the unconstrained and constrained ERT models in Figure 5. Lowering or increasing the layer resistivity by an order of magnitude (10 Ωm and 1000 Ωm , Models 2 and 4 in Table 1) results in large RRMS errors indicating disagreement between simulated and measured pseudosection. This shows that ERT is indeed sensitive to the order of magnitude of resistivity of this layer although it is not resolvable in a strict sense. The non-resolvability of thin layers, especially in greater depth, and the related ambiguity of the inversion results are well-known problems in ERT applications (e.g. Knödel *et al.*, 1997; Dahlin and Loke, 1998; Snieder, 1998). Nevertheless, the study shows that additional information from

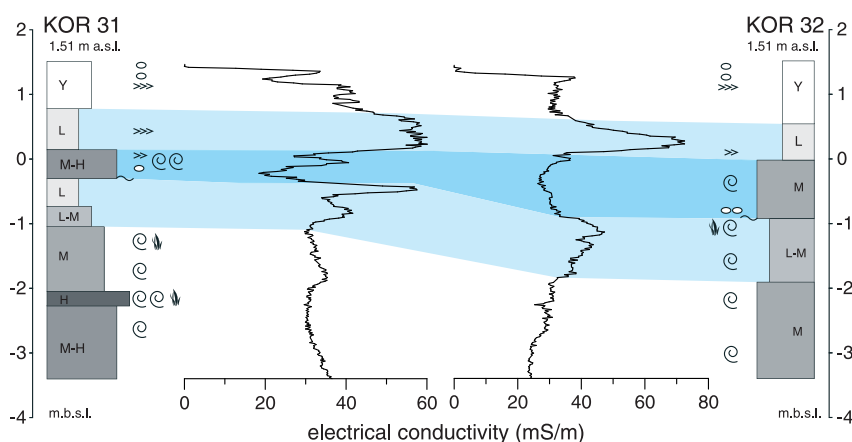


Figure 9. Stratigraphical composition and correlation of cores KOR 31 and KOR 32 based on field description and direct-push electrical conductivity (DP-EC) data obtained for both coring sites. DP-EC log data clearly document the lower and upper boundaries of the mid- to coarse-sand unit intercalating silt-dominated low-energy marine to lagoonal sediments (blue shading). The intercalating sand layer is characterized by clearly decreased electrical conductivity values. This example shows the enormous potential of a combined coring and DP-EC logging approach to improve our knowledge on stratigraphical issues. This figure is available in colour online at wileyonlinelibrary.com/journal/arp

DP-EC logs can be used as constraints for guiding ERT towards plausible solutions. To exactly verify the continuous gravel layer either more DP-EC logging or seismic measurements tracing the layer boundary would need to be performed.

The strong decrease of electrical resistivity at the depth level of the gravel layer (at coordinate $x = 60$ m in Figure 5b and 5c) could be explained in two ways: (1) by a local pinching out of the gravel layer, or (2) if the gravel layer is continuous, by the rise of (salty) water associated with the fault system. We favour the second explanation because gravel was found in each of the core drills in this study site and because a salt diapir is known to exist underneath the fault system (Fischer *et al.*, 2015).

Corfu City

The correlation of core KOR 31, DP KOR 31 and grain size data (Figure 6) yields detailed information on the sedimentary structure of the shallow subsurface. It is shown that DP-EC logs trace fluctuations in grain size at high resolution. These fluctuations can be interpreted as changes of depositional conditions in the course of time. High-energy input of marine sand, rich in shells and shell debris, at the base of the sequence is followed by low-energy deposits of lagoonal character. Depositional conditions then change again towards high- and medium-energy marine environments at a depth of 5.8 m b.s.l. before low-energy shallow marine to lagoonal conditions recur. Another intersection of marine sands rich in shell debris and

gravel was found at a depth around recent sea level. This change pattern in sedimentary environments is also reflected in core KOR 32 and the corresponding DP-EC log (Figure 9). The slight offset between core stratigraphical composition, DP-EC data and grain sizes is due to different compaction rates of the sediments during the drilling process and the occurrence of core loss or collapse material in drill holes without casing. In contrast, the electrical conductivity probe delivers continuous data for the entire sedimentary sequence.

For the lower part of the DP-EC log, where no core data are available, we detected a shift towards fine-grained, most likely silt and clay dominated deposits with high rates of penetration. Further cores drilled some 100 m to the south and 150 m to the northwest of sites KOR 31 and KOR 32, not presented in this paper, revealed that the shift towards high conductivity values correlated with thick deposits of silt-dominated lagoonal mud.

ERT cannot provide as detailed information about electrical resistivity as the DP-EC logs. Therefore, the incorporation of centimetres-scale thin layers as constraints of the ERT inversion does not make sense and might even lead to data artefacts. To avoid this, we used a simplified layer model based on stratigraphy from cores and mean resistivities from the DP-EC logs (Figures 7, 8). The variations of resistivity inside these layers, as seen in the trends of the electrical conductivity logs, is then accounted for by the 'permission' of the resistivity values to deviate from the given mean starting value to a certain predefined degree.

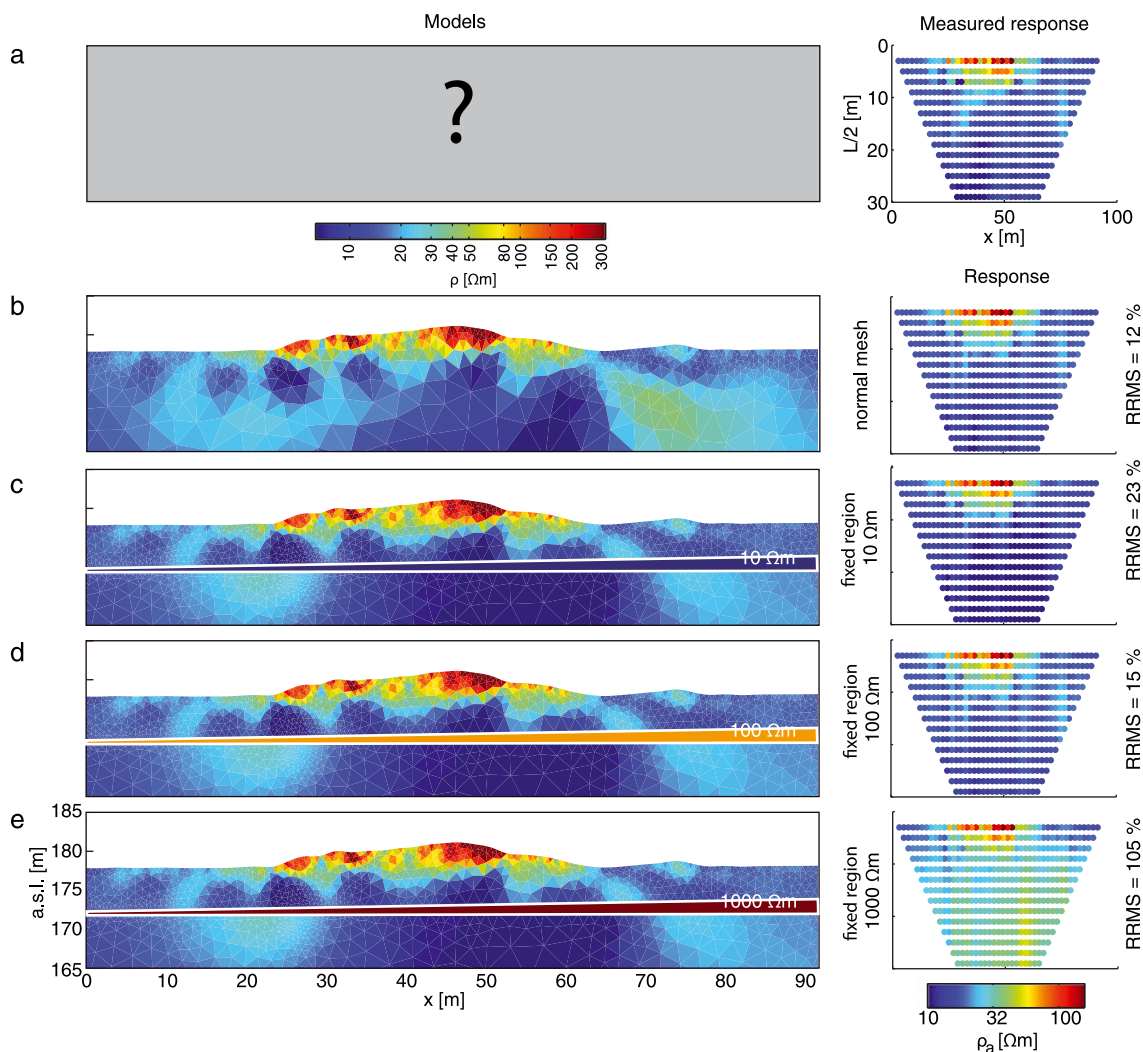


Figure 10. Comparison of measured and simulated apparent resistivity pseudosections (called 'response', right column) for different subsurface models (left column). From top to bottom: Measured field data (HOL ERT 18 transect), simulated data for unconstrained ERT model (Figure 5a), unconstrained ERT model with thin layer of constant resistivity of 10, 100 and 1000 Ωm in approximately 4 to 5 m depth corresponding to gravel layer in question. Note: ρ_a represents the apparent resistivity, L is the distance between the current electrodes of the ERT measurements, $L/2$ is a rough estimate of current penetration depth. RRMS is the relative root-mean-square difference (in %) between the apparent resistivity values of the measured and simulated pseudosections. This figure is available in colour online at wileyonlinelibrary.com/journal/arp

Table 1. Relative root mean square (RRMS) errors between the measured and simulated pseudosections of the subsurface resistivity models shown in Figure 10.

Model number	Model	Electrical resistivity of thin layer (Ωm)	RRMS error with respect to field data (%)
1	Unconstrained ERT model (Figure 5a)	n.a.	12
2	Model 1 plus thin layer	10	23
3	Model 1 plus thin layer	100	15
4	Model 1 plus thin layer	1000	105

The Corfu example illustrates that ERT can be improved by applying stratigraphic and resistivity constraints based on DP-EC logging. It shows also that stratigraphic constraints alone – which could be derived from coring without DP-EC logging – do not help in the case of laterally varying geoelectric structure. Using only layer interface depths as constraints, the ERT computation might even be misled and produce artificially high or low anomalies. This problem is overcome by using additional constraints on the electrical resistivity. Therefore, the accuracy of ERT profiling at the earth's surface can be considerably improved by increasing the number of DP-EC logs.

General discussion

Results presented here originate from two study sites which are characterized by a relatively homogeneous structure of the shallow subsurface. The integration of coring data and DP-EC logs showed that the ERT results can be improved by applying stratigraphic constraints and constraints of electrical resistivity to the inversion. Nevertheless, it becomes apparent that investigations in other settings which might be characterized by a more complex stratigraphy have to be based on more DP-EC logs as the quality of the calibration is dependent on the density of these point data. Applying ERT and DP-EC logging prior to coring will allow for reducing the number of sediment cores as relevant changes in the shallow subsurface are clearly visible in the DP-EC logs. In addition, the data set could even be extended by other geophysical methods, e.g. seismic profiling or ground penetrating radar, in order to create a more comprehensive picture of the shallow subsurface.

Conclusions

The results presented in this paper show the great potential of combining ERT measurements, DP-EC logs and core data.

The application of DP-EC logging allows for stratigraphical characterization of the shallow subsurface at higher resolution compared to coring and yield valuable data to calibrate ERT measurements. Based on the correlation with grain size data, it was shown that electrical conductivity logging accurately detects changes in sedimentary composition even in the saturated zone. Thus, if lithological or sedimentary units are once defined by the combination of coring and DP-EC logging, they can easily be traced over great distances using the DP-EC technique. A great advantage of this technique is, beside the robustness of the probe itself, the higher speed compared to standard coring. Especially in non-cohesive sediments, where boreholes tend to collapse if no casing is used, the direct-push technique allows investigation of the subsurface into greater depths.

The field examples showed that ERT profiling can be improved by applying stratigraphic constraints and constraints of electric resistivity to the ERT computations. Combining DP-EC and ERT in this way reduces the ambiguity of ERT results and leads to a more reliable interpolation of DP-EC based depth profiles. However, the Corfu example showed that stratigraphic information from coring alone (without DP-

EC) may be not sufficient for constraining or calibrating ERT in case of laterally varying structure.

Based on the presented examples we suggest the combined application of coring, DP-EC logging and ERT measurements as a standard tool for a comprehensive stratigraphical characterization of the shallow subsurface in geoarchaeological studies. Thereby, the spatial resolution of DP-EC logs and cores should be enlarged with increasing complexity of the stratigraphy.

Acknowledgements

Studies at the Holsterburg site were conducted in co-operation with the LVR-Amt für Bodendenkmalpflege and the Landschaftsverband Westfalen-Lippe (LWL). The authors are grateful for funding by the Ministerium für Bauen, Wohnen, Stadtentwicklung und Verkehr des Landes Nordrhein-Westfalen (North Rhine-Westphalia). The authors would like to thank Dr. Hans-Werner Peine and the whole excavation team of the LWL for support during field work. Studies in Corfu City are based on a long-term joint venture between the 8th Ephorate of Prehistoric and Classical Antiquities, the Greek Ministry of Culture and our research group. Based on this collaboration, detailed investigations within archaeological protection zones could be realized for which the authors are grateful. The German Research Foundation (DFG) is greatly acknowledged for funding (FI 1941/4-1, VO 938/22-1).

References

- Ad-hoc-AG Boden. 2005. *Bodenkundliche Kartieranleitung*, 5th edn. Ad-hoc-AG Boden: Hannover.
- Baika K. 2014. Corcyra (Corfu). In *Ships of the Ancient Mediterranean*, Blackman D, Rankov B, Baik K, Gerding H, Pakkanen J (eds)(eds). Cambridge University Press: Cambridge; 319–334.
- Bulla A, Knepe C. 2011. Die Holsterburg – eine oktagonale stauferzeitliche Buranlage bei Warburg. *Archäologie in Westfalen-Lippe* **2010**: 145–149.
- Bursian C. 1872. *Geographie von Griechenland*. Zweiter Band: Peloponnesos und Inseln. Leipzig.
- Dahlin T, Loke MH. 1998. Resolution of 2D Wenner resistivity imaging as assessed by numerical modelling. *Journal of Applied Geophysics* **38**: 237–249.
- DIN ISO 11277. 2002. *Bodenbeschaffenheit – Bestimmung der Partikelgrößenverteilung in Mineralböden – Verfahren mittels Siebung und Sedimentation*, ISO 11277:1998 and ISO 11277, Corrigendum 1. Beuth Verlag GmbH: Berlin.
- Direct Image. 2008. *Electrical Conductivity (EC) Logging. Standard Operating Procedure*. Direct Image: Salina, KS.
- Fischer P, Meurers-Balke J, Gerlach R, Bulla A, Peine, et al. 2015. Accepted for publication. Geoarchaeological and archaeobotanical investigations in the environs of the

- Holsterburg lowland castle (North Rhine-Westphalia) – evidence of landscape changes and saltwater upwelling. *Zeitschrift für Geomorphologie*. N.F. Supplementary Issue. http://dx.doi.org/10.1127/zfg_suppl/2015/S-00186
- Foley SF, Gronenborn D, Andreae MO, et al. 2013. The Palaeoanthropocene – the beginnings of anthropogenic environmental change. *Anthropocene* 3: 83–88.
- Günther T, Rücker C. 2006. A general approach for introducing information into inversion and examples from DC resistivity inversion. Extended Abstract. In *Proceedings, EAGE Near Surface*, September 4–6, Helsinki, Finland.
- Günther T, Rücker C, Spitzer K. 2006. Three-dimensional modelling and inversion of dc resistivity data incorporating topography – II. Inversion. *Geophysical Journal International* 166: 506–517.
- Harrington GA, Hendry MJ. 2006. Using Direct-Push EC Logging to delineate heterogeneity in a clay-rich aquitard. *Ground Water Monitoring & Remediation* 26(1): 92–100.
- Hausmann J. 2013. Parameterisation of the Near Surface by Combined Geophysical and Direct Push Techniques in the Frame of Geotechnical Site Investigation, PhD Thesis. Tübingen.
- Hecht S, Fassbinder J. 2006. Der Blick in den Untergrund: Magnetometrie und Geoelektrische Tomographie in der Geoarchäologie. *Geographische Rundschau* 58(4): 38–45.
- Knödel K, Krummel H, Lange G. 1997. *Handbuch zur Erkundung des Untergrundes von Deponien und Altlasten, Band 3, Geophysik*. Springer: Berlin.
- Meiburg P. 1982. Saxonische Tektonik und Schollenkinematik am Ostrand des Rheinischen Massivs. *Geotektonische Forschungen* 62: 1–267.
- Meurers-Balke J, Gerlach R, Fischer P, Vött A. 2014. Der Baugrund der Holsterburg und deren Umfeld. *Archäologie in Westfalen-Lippe* 2013: 125–129.
- Partsch J. 1887. Die Insel Korfu. Eine geographische Monographie. *Petermanns Mitteilungen, Ergänzungsheft* 88.
- Poulos SE, Lykousis V, Collins MB, Rohling EJ, Pattiaratchi CB. 1999. Sedimentation processes in a tectonically active environment: the Kerkyra-Kefalonia submarine valley system (NE Ionian Sea). *Marine Geology* 160: 25–44.
- Rabbel W, Erkul E, Stümpel H, et al. 2015. Discovery of a Byzantine Church in Iznik/Nicaea, Turkey: an educational case history of geophysical prospecting with combined methods in urban areas. *Archaeological Prospection* 22(1): 1–20.
- Sachpazi M, Hirn A, Clément C, et al. 2000. Western Hellenic subduction and Cephalonia Transform: local earthquakes and plate transport and strain. *Tectonophysics* 319: 301–319.
- Schön JH. 2004. Physical properties of rocks: fundamentals and principles of petrophysics. In *Handbook of Geophysical Exploration* 18, Helbig K, Treitel S (eds)(eds). Elsevier: Amsterdam; 583 pp.
- Schulmeister MK, Butler JJ Jr, Healey JM, et al. 2003. Direct-push electrical conductivity logging for high-resolution hydrostratigraphic characterization. *Ground Water Monitoring & Remediation* 23(3): 52–62.
- Seeliger M, Bartz M, Erkul E, et al. 2013. Taken from the sea, reclaimed by the sea: the fate of the closed harbor of Elaia, the maritime satellite city of Pergamon (Turkey). *Quaternary International* 312: 70–83.
- Snieder R. 1998. The role of nonlinearity in inverse problems. *Inverse Problems* 14: 387–404.
- Welham K, Fleisher J, Cheetham H, Manley H, Steele C, Wynne-Jones S. 2014. Geophysical survey in Sub-Saharan Africa: magnetic and electromagnetic investigation of the UNESCO World Heritage Site of Songo Mnara, Tanzania. *Archaeological Prospection* 21: 255–262.
- Wunderlich T, Petersen H, Attia al Hagrey S, Rabbel W. 2013. Pedophysical models for resistivity and permittivity of partially water-saturated soils. *Vadose Zone Journal* 12(4): . DOI:10.2136/vzj2013.01.0023.